Published paper:

M. Martinović et al., "Influence of winding design on thermal dynamics of permanent magnet traction motor," *Power Electronics, Electrical Drives, Automation and Motion (SPEEDAM), 2014 International Symposium on*, Ischia, 2014, pp. 397-402.

http://dx.doi.org/10.1109/SPEEDAM.2014.6872026

Influence of Winding Design on Thermal Dynamics of Permanent Magnet Traction Motor

Marijan Martinović, Damir Žarko, Stjepan Stipetić, Tino Jerčić, Marinko Kovačić, Zlatko Hanić
University of Zagreb, Faculty of Electrical Engineering and Computing
Department of Electric Machines, Drives and Automation
Zagreb, Croatia
marijan.martinovic@fer.hr, damir.zarko@fer.hr, stjepan.stipetic@fer.hr, tino.jercic@fer.hr, marinko.kovacic@fer.hr, zlatko.hanic@fer.hr

Dave Staton
Motor Design Ltd
Ellesmere, Shropshire, UK
dave.staton@motor-design.com

***Abstract*— This paper presents summarized electromagnetic and thermal design of interior permanent magnet motor for a low-floor tram TMK 2200. Motor geometry is optimized for maximum torque density using differential evolution algorithm. The influences of winding configuration on power losses and thermal transients in the motor during one driving cycle of the tram have been analyzed. The results indicate that an optimal number of turns per slot and parallel paths can be found to yield minimum temperatures in various parts of the motor considering the intermittent character of the load.**

Keywords*— *electric tram, traction motor, permanent magnet synchronous motor, electromagnetic design, losses, thermal analysis, duty cycle, optimization

I. INTRODUCTION

The induction motor (IM) is the dominant type of motor for driving modern electric vehicles on tracks, namely trams and electric multiple units. Its main advantages are low cost, robustness and high reliability.

Boosting of efficiency in all types of electric drives in industry and transport has been made one of strategic goals of energy policy conducted in Europe, United States (US) and elsewhere. For instance, new efficiency standards introduced by IEC [1], [2] are targeted towards increase of efficiency of induction and other types of motors supplied from the mains or variable-speed drives which are sold on the European market. Similar standards (NEMA, EPACT, CSA, CEMEO etc.) exist in other parts of the world as well. The increase of efficiency can be achieved by increasing the size of existing motors and/or installing laminations with lower specific losses. Further improvement may be achieved with redesign of the geometry of existing motors by means of mathematical optimization.

In the case of traction drives, the limited space available on the bogie of a vehicle is always a restraining factor for the traction motor. In order to increase efficiency and maintain reasonable motor size, a synchronous motor with permanent magnets (SMPM) with its inherently higher torque density and better efficiency than induction motor is emerging as a solution [3],[4]. For traction applications interior permanent magnet (IPM) fits naturally due to its torque-speed characteristic suitable for wide speed range in constant power mode of operation which can be tuned as required by proper design of the motor.

Tariq *et. al.* [6] compared different IPM machine designs for torque-speed profile, efficiency and demagnetization limit at different current loading with increased machine cooling. Wang *et. al.* [7] researched the influence of PM temperature on performance of IPM traction motors. Rahman *et al.* [5] defined numerous requirements that an IPM traction motor must satisfy of which the following are in the focus of this research: high torque density, extended speed range, effective cooling, safety and reliability.

In order to meet all requirements mentioned above in the design stage, a need for combined thermal, electromagnetic and mechanical analysis of the machine arises. Selection of the appropriate type of magnets and winding insulation class are strongly temperature dependent leading to a conclusion that thermal analysis is of equal importance as electromagnetic analysis, while mechanical analysis provides warranty of safety and reliability at maximum speed.

This paper studies the possibility of replacing an existing induction motor driving a low floor tram TMK2200 manufactured by Crotram consortium with an IPM motor of the same volume, but with increased torque rating so that six induction motors can be replaced with four IPMs.

Special emphasis is made on influence of winding design on thermal dynamics of the motor. The selected number of turns per coil and the number of parallel paths determines the speed at which traction motor enters the field weakening regime which affects the distribution of copper and iron losses in the motor as a function of tram (motor) speed. As a consequence the maximum temperature reached in the various parts of the motor during one driving cycle of the tram (acceleration → constant speed → braking → standstill) is dependent on the winding design. The detailed results of thermal analysis are presented in the paper suggesting the best choice for winding design in this particular case.

Goss *et. al.* [8] proposed a design methodology for PM AC traction motor. They considered combined electromagnetic, thermal and mechanical performance. The problem of the winding design (number of turns per coil) emerged also in their research. Nevertheless, the accent was put on thermally constrained continuous maximum torque (and power) envelope rather than on the losses and temperature in various active parts during complex duty cycle of IPM railway traction motor as in this paper.

All simulations in this paper are performed using SPEED PC-BDC+PC-FEA and Infolytica MagNet software for electromagnetic analysis, and Motor-CAD software for thermal analysis. The motor design process is further improved by applying evolutionary optimization implemented in MATLAB in combination with commercial SPEED PC-BDC+PC-FEA software.

II. Traction Motor requirements

An induction motor (IM) which drives low-floor tram TMK2200 is used in this research as a starting point for IPM motor design. The IM mounted on the tram bogie and on the test bed in the Laboratory of Electric Machines at the University of Zagreb is shown in Fig. 1. The main idea is to fit the IPM motor into the frame of the existing IM to permit assembly on the tram without additional modifications. Along with the assumption of identical dimensions of the frame, both machines are assumed to have the same shaft, bearings and cooling system which result in the same friction and windage losses.

Tramcar series TMK2200 is driven by six three-phase four pole squirrel cage induction motors with the following ratings for maximum load during acceleration: 85 kW, 320 V, 195 A, 477 Nm, 1700 min^{-1}. The maximum speed is 4580 min^{-1}. During regenerative braking the maximum developed torque is -680 Nm. The stator has form wound coils with insulation class 200. Mechanical protection is IP20 (open motor), so interior of the motor is exposed to outside moisture and dirt.

The torque requirements for IPM motors for the same performance of the tram will be 50 % higher since four motors will be used. The stator is assumed to have random wound coils made of round enameled wire with H class insulation and maximum allowed hot-spot temperature of 180 °C. During exploitation wheels of the tram are exposed to wear creating tiny iron particles that can stick to the rotor of the IPM motor due to attracting forces of the magnets. After a certain period of time it can fill the air gap and damage the motor. Therefore, the IPM motor needs to be built with IP55 degree of mechanical protection (totally enclosed).

Electromechanical requirements for the traction motor are determined by solving kinematic equations of the tram using the following data: mass of vehicle and passengers, maximum speed, maximum allowed acceleration and deceleration, maximum allowed acceleration time, maximum allowed path for stopping, wheel diameter and gearbox ratio. Based on the data found in literature [9], [10] and provided by the manufacturer of the tram, the traction force, acceleration, tram speed and motor torque shown in Figs. 2 to 4 have been calculated. The distance between two stations is 1000 m. A driving cycle consists of acceleration to the maximum speed of 70 km/h followed by driving at constant maximum speed and braking to standstill. The tram is idle for 20 seconds until the start of a new cycle.

The IPM motor must provide 705 Nm of torque during acceleration and 1020 Nm during braking.

III. Measured Characteristics of Existing Induction Motor

The friction and windage losses of the IPM motor and its through ventilation characteristic are assumed to be the same as in induction motor since both motors have the same bearings, cooling fan and geometry of cooling ducts.

The amount of friction and windage losses is measured on TMK 2200 induction motor in no-load test conducted according to IEC standard [11]. These losses shown in Fig. 5 are used for the purpose of the IPM motor design as an input to PC-BDC+PC-FEA software.

Since the induction motor forces air flow through axial cooling ducts via a shaft mounted fan, in order to define cooling performance of newly designed machine it is required to measure the air velocity in the ducts. Air velocity was measured using hot wire anemometer at a variety of rotor speeds in the ducts labeled according to Fig. 5. Cooling ducts were accessible for measurement only on the drive end of the motor since cooling fan is mounted on the rear making the openings of the ducts inaccessible.

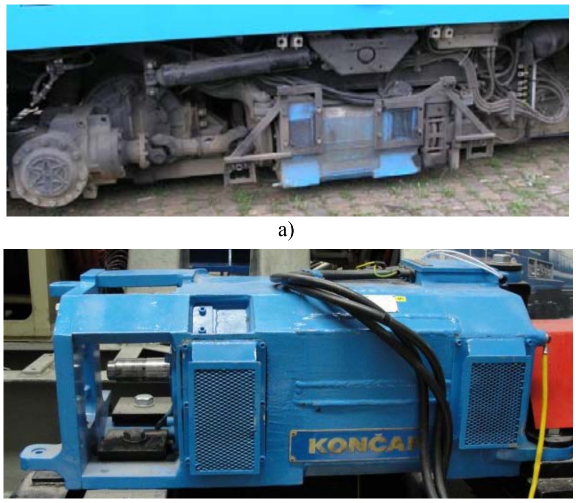

Fig. 1. Induction motor for low-floor tram TMK2200, a) mounted on the bogie, b) mounted on the test bed in the laboratory.

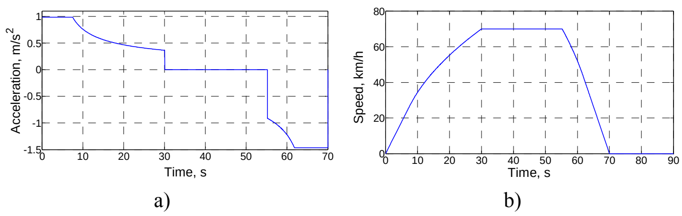

Fig. 2. Tram acceleration (a) and speed (b) versus time during one driving cycle.

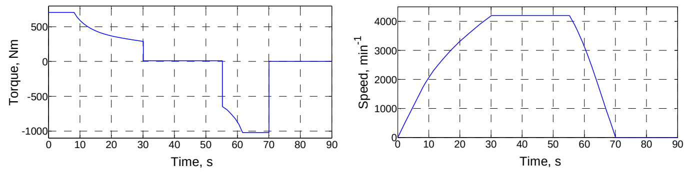

a) b)

Fig. 3. Required torque of IPM motor (a) and shaft speed (b) versus time during one driving cycle.

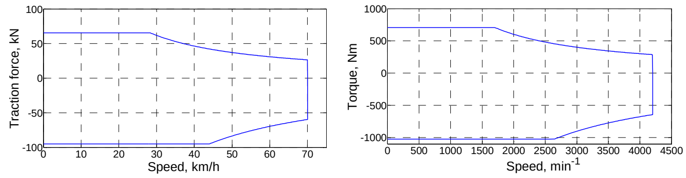

a) b)

Fig. 4. Traction force on the wheels (a) and required torque of IPM motor (b) versus speed during one driving cycle.

Due to uneven area of cooling ducts and their circumferential distribution on the perimeter of the stator laminations, the measured air velocity varies for different ducts. Hence, air velocity versus rotor speed is modeled as a red regression line shown in Fig. 5b. This characteristic is used as an input for thermal modeling of the IPM motor.

Another input to thermal model are power losses in the winding, core and permanent magnets of the motor, the amount of which depends on the duty cycle and required torque that traction motor must develop at a certain speed. With known driving conditions and tram specifications [10], the duty cycle of the tram can be determined and translated into the traction motor duty cycle in the form of required shaft torque and speed as a function of time as previously shown in Fig. 3.

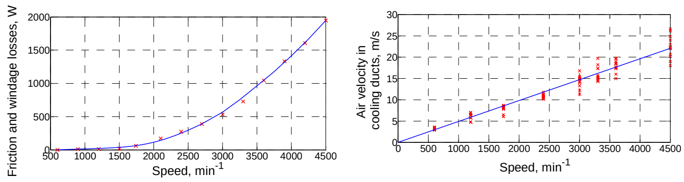

a) b)

Fig. 5. Measured friction and windage losses (a), and air velocity in cooling ducts (b) of induction motor.

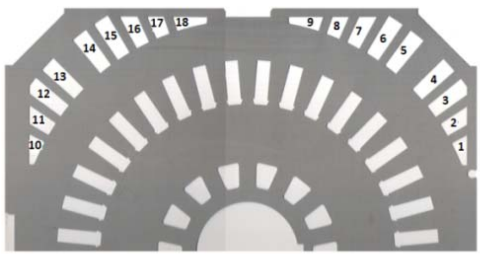

Fig. 6. Induction motor stator and rotor lamination with axial cooling ducts (rotor bar slots and air gap not yet punched).

IV. OPTIMIZED DESIGN OF IPM MOTOR

Design of a traction motor is more complex than design of a motor for continuous duty due to intermittent character of the load. Consideration of the entire driving cycle of the vehicle in terms of time dependence of generated power losses and the resulting heating of the motor is computationally too intensive. Therefore, the motor design is performed in two steps:

1) Optimization of radial cross-section by maximizing the torque density within predefined constraints,
2) Selection of number of turns per coil and number of parallel paths considering calculated thermal transient of the motor during one driving cycle.

The optimization of the motor design is realized using differential evolution (DE) algorithm [12], connecting SPEED PC-BDC software and MATLAB via ActiveX. In order to obtain reliable results, PC-FEA finite element (FE) module was used to take into account the influence of saturation on synchronous inductances in *d* and *q* axis.

Two sets of variables are defined. The first set are variables with constant values listed in TABLE II. which are not subject to optimization. The second set are variables listed in TABLE I. which are being optimized with respect to inequality constraints defined in TABLE II. and the cost function (torque density). The variables subject to optimization have been normalized in order to minimize the occurrence of unfeasible motor geometries that would frequently emerge otherwise.

The selected current density and the limit of linear current density equal the values used in the induction motor at maximum developed torque during acceleration of the tram. Since IPM motor is totally enclosed, in spite of the fact that its rotor losses are much smaller than rotor losses in the IM, it is expected that temperature of the rotor and permanent magnets will be high due to heat transfer from the stator and the fact that only stator surface is forced ventilated. Therefore, the selected NdFeB magnet type is N38EH for maximum temperature of 200 °C.

The number of slots and poles is selected to be 36/8 which yields a two-layer fractional slot winding with distributed overlapping coils and with good trade-off between inherent capability for mitigation of torque pulsations, susceptibility to noise and possibility of using multiple parallel paths.

Optimization resulted in a motor geometry with the highest torque within given stack volume which satisfies all constraints. The obtained torque density is 27.4 kNm/m^3. The radial view of the optimal lamination design and field plots from FE simulation at maximum torque during acceleration are shown in Figs. 7 and 8. Minor modifications of the shapes of permanent magnet cavities in the rotor have been made with respect to the output from PC-BDC in order to better secure the magnets in position. These modifications do not affect the electromagnetic properties of the optimal design.

Optimization was carried out with one turn per coil and one parallel path. If current density is kept the same, the subsequent variations in winding design do not affect the amount of torque the motor will developed since torque solely depends on total ampere-turns in the slot.

TABLE I. DEFINITION OF OPTIMIZATION VARIABLES

Term	Boundaries	Explanation
D_s/D_{so}	[0.45, 0.75]	Ratio of stator inner diameter (D_s) to outer diameter (D_{so})
$d_{ys}/[(D_{so}-D_s)/2]$	[0.3, 0.7]	Ratio of yoke thickness (d_{ys}) to difference between stator outer ($D_{so}/2$) and inner radius ($D_s/2$)
b_{ts}/τ_s	[0.3, 0.7]	Ratio of tooth width (b_{ts}) to slot pitch (τ_s) at D_s
$\lambda_m = d_m/[(D_r-D_{rin})/2]$	[0.1, 0.3]	Ratio of total cavity thickness (d_m) to difference between rotor outer ($D_r/2$) and inner radius ($D_{rin}/2$)
λ_{md1}	[0.2, 0.6]	Relative share of total rotor lamination depth for outermost rotor section
λ_{md2}	[0.05, 0.4]	Relative share of total rotor lamination depth for middle rotor section (between the cavities)
β/β_0	[0.7, 1]	Angle of slanted magnets (β) relative to maximum feasible angle (β_0)
λ_p	[0.55, 0.95]	Angular span of the inner rotor cavity relative to the pole pitch

TABLE II. IPM MOTOR CONSTANT GEOMETRIC PARAMETERS

Parameter	Value
Number of slots	36
Number of poles	8
Stator outer diameter, mm	320
Stack length, mm	320
Shaft diameter, mm	70
Air gap, mm	1
Slot opening width, mm	2,5
Slot opening depth, mm	1
Coil pitch	4
Slot fill factor	0,4
RMS current density, A/mm2	6.6
Permanent magnet type	NdFeB (N38EH)

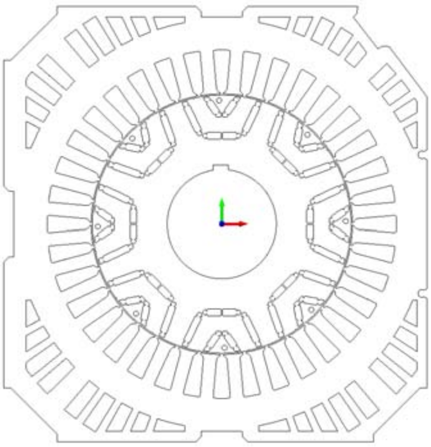

Fig. 7. Stator and rotor laminations of the final optimized design.

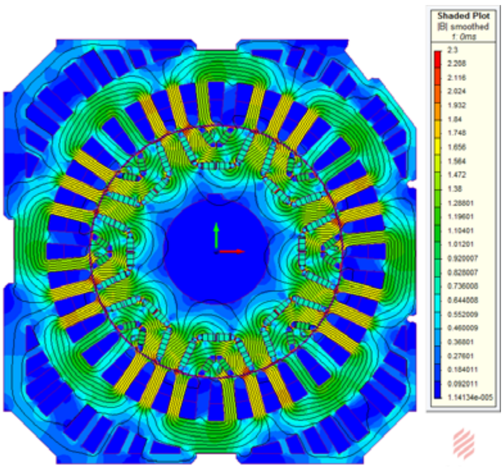

Fig. 8. Magnetic flux lines and flux density plot of the final optimized design.

TABLE III. IPM MOTOR INEQUALITY CONSTRAINTS

Parameter	Symbol	Constraints
RMS linear current density	K	$\leq$ 51.5 kA
Efficiency	η	$\geq$0.95 %
Power factor	cos φ	$\geq$ 0,8
Flux density in stator tooth	$B_{st,max}$	$\leq$1,8 T
Flux density in stator yoke	$B_{sy,max}$	$\leq$1,35
Power at maximal speed	$P_{@max\_speed(5100\ rpm)}$	$\geq P_{@rated\_speed(1700\ rpm)}$
Voltage at maximal speed	$U_{@max\_speed(5100\ rpm)}$	$\leq U_{@rated\_speed(1700\ rpm)}$

V. INFLUENCE OF REWINDING ON MACHINE PERFORMANCE

In order to fully utilize the available electromagnetic and reluctance torque, an optimum angle γ (Fig. 9) between phase current and back EMF should be maintained to achieve maximum torque per ampere (MTPA) operation up to corner speed at which maximum available voltage is reached. Above corner speed reduced torque operation is achieved by adjusting the current angle to weaken the magnet flux [13], [14]. The corner speed can be changed by altering the number of turns per coil (N_c) and the number of parallel paths (a_p). This variation also affects losses in the machine generated during the driving cycle of the vehicle.

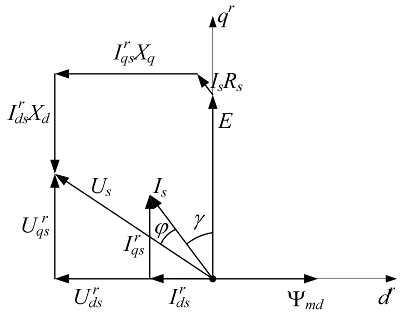

Fig. 9. Phasor diagram of IPM motor.

Reducing the ratio N_c/a_p reduces the back EMF E which entails decrease of the total phase voltage U_s at a certain speed. In that case the transition to the flux weakening regime is shifted to a higher speed. The constant power speed ratio (CPSR) of the motor is not affected by rewinding of the motor [15]. It is an inherent property of the motor determined by geometric design of its cross-section, current density and magnetic properties of laminations and permanent magnets which all affect the level of saturation and motor parameters that define the CPSR. Therefore, the CPSR obtained by optimized design will be preserved.

Since total quantity of copper in the slots remains unchanged (slot fill factor is fixed), reducing N_c/a_p increases the diameter of a conductor. In that case a reduction of N_c/a_p yields a proportional increase of the phase current to ensure the same current density, MMF and torque. This is valid in constant torque regime.

In traction applications the transition from constant torque to constant power region is determined by vehicle kinematics and is not necessarily followed by traction motor design. In other words, the starting point of flux weakening regime of the motor defined by the value of torque and speed at which maximum available voltage from the power converter is reached usually occurs at speeds higher than the speed at which constant traction power regime begins. In this particular case Fig. 4 indicates that constant traction power begins at tram speed of 28 km/h, which corresponds to motor speed of 1700 min^{-1}. However, the selection of ratio N_c/a_p will determine the speed at which maximum available voltage will be reached. The motor will develop constant power starting from 1700 min^{-1}, but this regime will be maintained by reducing the motor current and increasing the motor voltage up to the speed at which maximum available voltage is reached. In this interval the current control angle γ will still be kept at a value that yields maximum torque per ampere. Beyond that speed the current angle will be continuously increased thus weakening the motor flux up to maximum tram speed.

In constant torque regime up to 1700 min^{-1} the current density, copper losses and iron losses will be the same regardless of the N_c/a_p ratio. However, in constant power regime the rate of change of current density and flux with speed will be dependent on N_c/a_p. Consequently, the copper and iron losses will also be dependent on N_c/a_p as the speed increases. It should be noted that motor needs to develop the same torque in the entire speed range regardless of the N_c/a_p ratio, because torque reference is governed by traction force requirement of the tram.

The described principle is demonstrated for three winding configurations: a) **5** turns per coil, **4** parallel paths, b) **6** turns per coil, **4** parallel paths, c) **7** turns per coil, **4** parallel paths. The second winding is equivalent to the winding with 3 turns per coil and 2 parallel paths.

The developed torque, voltage, line current, current density and power losses versus speed during acceleration for all three cases are compared in Figs. 10 and 11. Similar dependence can be obtained for regenerative braking regime as well, only in this case higher voltage limit of 520 V on the motor terminals is allowed. It is important to notice that motor with 7 turns needs the lowest current in constant torque regime which is beneficial from the aspect of power converter design and efficiency since at lower current, conducting and switching losses are lower as well. In addition, depending on standard ratings of IGBT's available on the market, in some cases significant cost reduction may be achieved if IGBTs will lower current rating may be installed. Although with further increase of N_c/a_p the motor current in constant torque regime will decrease, the current density and winding losses in constant power regime will increase, inevitably leading to increase of maximum temperatures in the motor. This happens because winding configurations with higher N_c/a_p enter the flux weakening regime at lower speed and hence demagnetizing (d-axis) component of MMF is higher than in windings with lower N_c/a_p resulting in higher current density.

Above the speed (approx. 3500 min^{-1}) at which all three winding configurations are in the flux weakening regime (voltage limit of 400 V is reached) the line current is the same (Fig. 10). This is logical since at constant power and constant voltage the same current is required if power factor and efficiency are the same.

In order to find the winding configuration with best thermal performance (lowest temperatures), the variations of power losses in various parts of the motor are calculated as a function of time during one driving cycle and used as input to the thermal model. All time dependent waveforms are shown in Figs. 12 to 15. Friction and windage losses (Fig. 15), which are modeled in SPEED based on measured results, depend only on rotor speed and not on winding variation.

A motor with lower N_c/a_p reaches the flux-weakening region at a higher speed resulting in higher motor flux and higher stator iron losses (Fig. 14a). On the contrary, rotor iron losses, which occur due to higher order harmonics of stator MMF, decrease for lower N_c/a_p due to lower current density and hence lower MMF (Fig. 14b).

The results of transient thermal simulations, shown in Figs. 16 and 17, indicate that winding with 6 turns per coil and 4 parallel paths reaches the lowest overall temperatures. This winding is the best choice from the aspect of motor efficiency and thermal stress considering intermittent character of the load during one driving cycle of the tram.

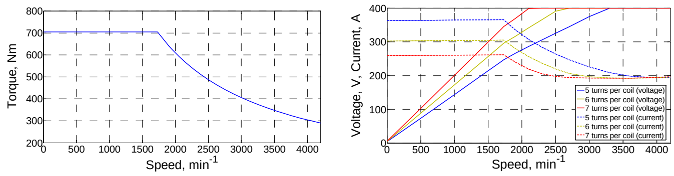

a) b)

Fig. 10. Shaft torque (a), terminal voltage and line current (b) versus speed during acceleration for all three winding configurations

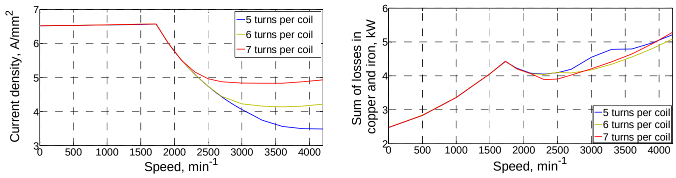

a) b)

Fig. 11. Current density (a) and total power losses (b) versus speed during acceleration for all three winding configurations

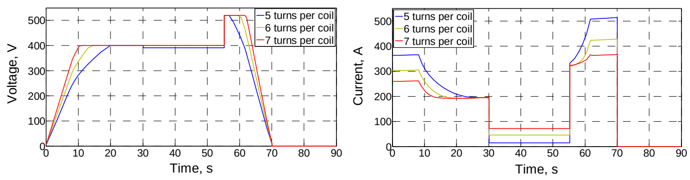

a) b)

Fig. 12. Terminal voltage (a), and line current (b) versus time during one driving cycle.

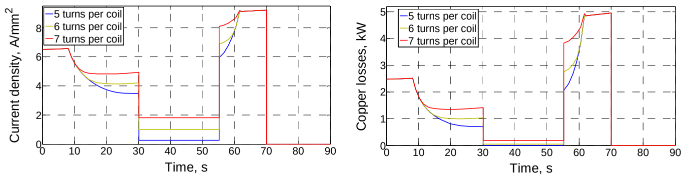

a) b)

Fig. 13. Current density (a) and copper losses (b) versus time during one driving cycle.

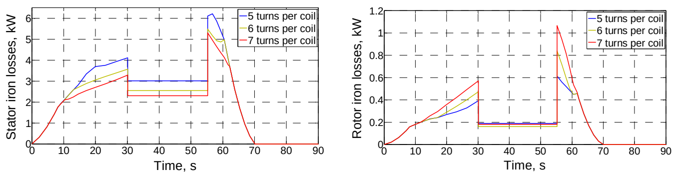

a) b)

Fig. 14. Stator (a) and rotor (b) iron losses versus time during one driving cycle.

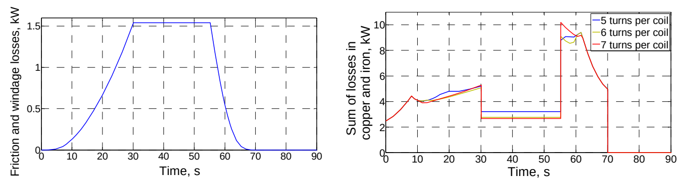

a) b)

Fig. 15. Friction and windage losses (a) and total losses (b) versus time during one driving cycle.

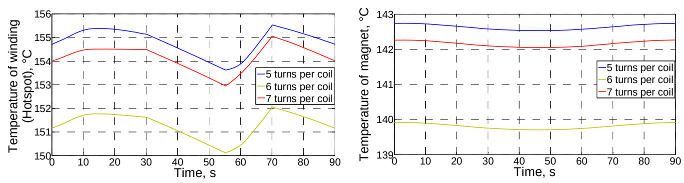

a) b)

Fig. 16. Winding (a) and permanent magnet (b) temperature versus time during one driving cycle.

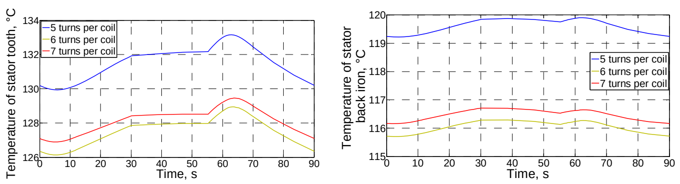

a) b)

Fig. 17. Stator tooth (a) and stator back iron (b) temperature versus time during one driving cycle.

VI. Conclusion

The analysis of influence of winding configuration on thermal transients of an IPM traction motor during one driving cycle of an electric tram shows that winding configuration primarily affects the power losses in the constant traction power regime. Therefore, it is possible to find the number of turns per coil and the number of parallel paths that yield the lowest temperatures in various regions of the motor. The winding configuration also affects the current rating of the power converter, so in order to assess the trade-offs in efficiency and cost of the entire traction drive, similar analysis would have to be conducted for the power converter as well before final conclusion can be made on the best winding configuration for the motor.

Acknowledgment

This research if funded by European Union under the project titled *Permanent Magnet Machine Technology for Boosting the Energy Efficiency in Traction and Marine Applications* (MAGEF), Contract No. IPA2007/HR/16IPO/001-040508. The purpose of this project is to enhance the capability of University of Zagreb for research and development of PM machines for applications in transport, power engineering and industry. The authors also thank the project associate Končar Electric Vehicles Inc., Croatia for providing valuable data on TMK2200 tram.

References

[1] IEC 60034-30 Ed. 1: Rotating electrical machines - Part 30: Efficiency classes of single speed, three-phase, cage induction motor (IE Code), International Electrotechnical Comission (IEC), 2008

[2] IEC 60034-31: Rotating electrical machines - Part 31: Guide for the selection and application of energy-efficient motors including variable-speed applications, International Electrotechnical Comission (IEC), 2009

[3] A. M. El-Refaie, "Motors/Generators for Traction/Propulsion Applications: A Review." *IEEE Vehicular Technology Magazine* 8, no. 1 (2013).

[4] M. Mermet-Guyennet, "New power technologies for traction drives." *Power Electronics Electrical Drives Automation and Motion (SPEEDAM), 2010 International Symposium on*, pp. 719-723. IEEE, 2010.

[5] Z. Rahman, M. Ehsani, K. L. Butler. "An investigation of electric motor drive characteristics for EV and HEV propulsion systems." *SAE transactions* 109, no. 6 (2000): 2396-2403.

[6] A. R. Tariq, C. E. Nino, E. G. Strangas. "Effect of cooling conditions on the design and operation of IPMSM." *Power & Energy Society General Meeting, 2009. PES'09. IEEE*, pp. 1-10. IEEE, 2009.

[7] A. Wang, L. Heming, C. T. Liu. "On the material and temperature impacts of interior permanent magnet machine for electric vehicle applications." *Magnetics, IEEE Transactions on* 44, no. 11 (2008): 4329-4332.

[8] J. Goss *et. al.*, "The design of AC permanent magnet motors for electric vehicles: A design methodology," *Electric Machines & Drives Conference (IEMDC), 2013 IEEE International* , vol., no., pp.871-878, 12-15 May 2013

[9] D. Krušelj, J. Ungarov, V. Siladi, "Direct Torque Control of Induction Motors with Stator Flux Correction Applied to the Low-floor Tramcars." *AUTOMATIKA: časopis za automatiku, mjerenje, elektroniku, računarstvo i komunikacije* 48, no. 3-4 (2007): 85-98.

[10] KONČAR TMK2200 and TMK2200-K low-floor tramcar brochure, http://www.koncar-kev.hr/docs/koncarkevEN/documents/15/2_1/Original.pdf

[11] IEC 60034-2-1: Rotating electrical machines –Part 2-1: Standard methods for determining losses and efficiency from tests (excluding machines for traction vehicles), International Electrotechnical Comission (IEC), 2009

[12] K. Price, R. Storn, *Differential Evolution - A Practical Approach to Global Optimization*, Springer, Berlin, 2005.

[13] B. Sneyers, D. W. Novotny, T. A. Lipo, "Field Weakening in Buried Permanent Magnet AC Motor Drives," *Industry Applications, IEEE Transactions on* , vol.IA-21, no.2, pp.398-407, March 1985

[14] T. M. Jahns, "Flux-Weakening Regime Operation of an Interior Permanent-Magnet Synchronous Motor Drive," *Industry Applications, IEEE Transactions on* , vol.IA-23, no.4, pp.681-689, July 1987

[15] D. Žarko, S. Stipetić, "Criteria for Optimal Design of Interior Permanent Magnet Motor Series," XXth International Conference on Electrical Machines (ICEM' 2012), pp. 1242-1249, Marseille, France, September 2-5, 2012